LETTERS

Computer simulation of high-temperature, forsterite-melt partitioning

JOHN A. PURTON,[1,2,]* JON D. BLUNDY,[1] AND NEIL L. ALLAN[2,]†

[1] CETSEI, Department of Earth Sciences, University of Bristol, Bristol BS8 1RJ, U.K.
[2] School of Chemistry, Cantock's Close, University of Bristol, Bristol BS8 1TS, U.K.

ABSTRACT

We report the first atomistic computer simulations of the partitioning of divalent cations between forsterite (Mg_2SiO_4) and coexisting $MgSiO_3$ melt at ~1600 °C and atmospheric pressure. Our results, using new Monte Carlo techniques, are compared with new experimental determinations of forsterite-melt partitioning for the same elements (Ca, Mn, Ni, Co, Cu, Zn, Sr, Cd, Ba) in the same system under identical conditions. Over seven orders-of-magnitude variation in the Nernst partition coefficient (D), experiment and simulation agree typically within a factor of 2 and at worst to within a factor of 4.2 (D_{Sr}). Our simulation techniques therefore herald a novel means of determining crystal-melt partitioning that may be especially valuable under extreme conditions of pressure and temperature not readily amenable to experimentation.

INTRODUCTION

Our knowledge of the accretion and subsequent chemical differentiation of the Earth derives largely from chemical analyses of trace elements and their isotopes in rocks. Modeling and interpretation of these data require an understanding of how trace elements are partitioned between coexisting phases. Of particular importance is the case of crystal-melt partitioning of trace elements (<0.1% by weight) in magma at high temperatures. Such information is conventionally determined either by high-temperature experiments, or by analysis of porphyritic volcanic rocks.

Trace-element partitioning is a thermodynamic process controlled by the energetics of incorporation of elements at the part per million (ppm) level into coexisting phases. Nernst partition coefficients (D, defined as the weight concentration ratio crystal/melt) vary greatly between crystal phases and between different trace elements. At a fixed temperature and pressure, the variables that exert the most control over partitioning are the charge and size of the substituent ion, and the atomic structure of the coexisting phases (Goldschmidt 1937). Incorporation of defect cations into any phase involves the making and breaking of chemical bonds and the subsequent distortion (or relaxation) of the structure to accommodate the misfit in size and/or charge. As crystals have more rigid structures than silicate melts, the relaxation energy in the crystal typically dominates the partition coefficient (Purton et al. 1996). Recently, Blundy and Wood (1994) and Beattie (1994), building upon earlier works (Nagasawa 1966; Brice 1975), developed empirical lattice strain models for relaxation in the solid phase based upon the size mismatch between the substituent cation and the lattice site of interest. The model of Blundy and Wood

(1994) describes partitioning of a cation, i, with radius r_i, onto a lattice site in terms of three parameters: r_0, the optimum radius of the site (r_i-r_0 is then a measure of size mismatch); E, the apparent Young's Modulus of the site (a description of the elastic response of the lattice around the site); and D_0, a strain-free partition coefficient for an ion of radius r_0. These models have since been widely used to rationalize trace-element partitioning in a large number of silicate mineral phases (e.g., Brenan et al. 1995; Wood and Blundy 1997; Klein et al. 1997; Lundstrom et al. 1998; Taura et al. 1998; Van Westrenen et al. 1999). These empirical models employ a simplified description of elastic strains in isotropic crystal lattices. Such strains are also calculable through atomistic computer simulations, which afford atom-scale insights that are beyond the resolution of current experimental techniques. In earlier work (Purton et al. 1996, 1997a), we carried out point-defect calculations at constant volume for the solid phase in the static limit (i.e., $T = 0$ K, and ignoring lattice vibrations) for a wide range of substituents. We have thus been able to link continuum theory and simulation to investigate the success of the empirical models for the relaxation energy. In addition, calculated substitution (solution) energies, obtained from a combination of defect energies and lattice energies of the relevant binary oxides, usually show the same qualitative trends with ionic radius as the experimentally determined partition coefficients for the phases studied so far (Purton et al. 1997a). However, for computer simulations to be directly applicable to crystal-melt partitioning it is necessary to incorporate the effects of both temperature and the melt phase. This requires development of new simulation techniques that take account, among other things, of vibrational effects at high temperature, and the disorder in the melt. Here we present a new Monte Carlo technique for this purpose.

COMPUTER SIMULATION

Monte Carlo (MC) calculations were carried out at constant temperature (1600 °C) and pressure (0.1 MPa), allowing aniso-

---

*Present address: CLRC, Daresbury Laboratory, Warrington, Cheshire WA4 4AD, U.K.
†E-mail: n.l.allan@bris.ac.uk

tropic deformations of the unit cell of the solid. During an MC cycle, one of two options is chosen at random. Either the atomic co-ordinates of a randomly chosen atom are allowed to vary by making a random move of that atom in the range $[-r_{max}, r_{max}]$, or a random change in the volume/shape of the box (Frenkel and Smit 1997) in the range $[-V_{max}, V_{max}]$ is attempted. In each case the Metropolis algorithm (Metropolis et al. 1953) is applied to determine whether or not the change is accepted. For each atomic species, r_{max} (and V_{max}) is chosen such that there are equal numbers of accepted and rejected trials. The potential model employed and its transferability from one silicate to another has been discussed previously (Catlow and Price 1990, and references therein); the set of short-range potential parameters is given in Table 1. For the solid phase, the simulations were carried out using 896 atoms ($2 \times 4 \times 4$ unit cells of forsterite), in which one Mg^{2+} ion was replaced by a single trace-element cation, i^{2+}. Enthalpy and structural data were averaged over a period of 10^8 cycles (1 cycle equals a random move or volume change), prior to which an equilibration period of 10^8 cycles was undertaken. A few runs with a larger cell of 1344 ions gave almost identical results. In our simulations at 1600 °C the cations in the solid phase are mobile (i.e., pre-melting has occurred) so that the M1 and M2 sites are indistinguishable. A recent in-situ neutron diffraction study of Fe-Mn and Mg-Mn olivines (Redfern et al. 1997) confirms that they approach complete M-site disorder at $T \approx 1600–1700$ °C.

The binary phase diagram of the $MgO-SiO_2$ system at 0.1 MPa (Bowen and Andersen 1914) indicates that at 1600 °C forsterite is in equilibrium with a melt composition of ~60 wt% SiO_2. Hence calculations for the melt started assuming an enstatitic ($MgSiO_3$) structure. The simulation box of 1200 atoms was "heated" until the structure had melted, as determined from the mobility of the ions. The resulting structure was used for subsequent calculations in which one i^{2+} replaced one Mg^{2+}. The number of equilibration and data collection cycles were the same as for the solid phase.

The calculations relate to the enthalpy change (ΔH_{ex}) for exchange equilibria of the type:

$$Mg_2SiO_4 \text{ (crystal)} + iSiO_3 \text{ (melt)} = \quad (1)$$
$$iMgSiO_4 \text{ (crystal)} + MgSiO_3 \text{ (melt)}$$

The equilibrium constant for this reaction is:

$$K_d^{i-Mg} = \frac{a_{iMgSiO_4}^{crystal} a_{MgSiO_3}^{melt}}{a_{iSiO_3}^{melt} a_{Mg_2SiO_4}^{crystal}} = \exp\left(\frac{-\Delta G_{ex}}{RT}\right) \quad (2)$$

where ΔG_{ex} is the free energy change of reaction 1 at the pressure (P) and temperature (T) of interest, and R is the gas constant. Taking as our standard state i^{2+} infinitely dilute in forsterite and melt, and assuming that: (1) the octahedral cations in the crystal and melt are disordered at high T (Redfern et al. 1997); (2) the entropy change for reaction 1 is negligible as indicated by the similar entropies of fusion of Mg, Fe, and Mn olivines (Hirschmann and Ghiorso 1994); and (3) the difference in molecular weight between crystal and melt is very small, Equation 2 reduces to:

$$K_d^{i-Mg} = \frac{X_i^{crystal} X_{Mg}^{melt}}{X_i^{melt} X_{Mg}^{crystal}} = \frac{D_i}{D_{Mg}} = \exp\left(\frac{-\Delta H_{ex}}{RT}\right) \quad (3)$$

where D_i denotes the partition coefficient for i^{2+}. In the simulations D_{Mg} is 1.43 (by definition), hence Equation 3 can be used to calculate D_i from ΔH_{ex} for each of the simulated species (Table 2).

EXPERIMENT

To test our calculated partition coefficients we have performed experiments under conditions identical to those in the simulations. Experimental starting materials were sintered powders of MgO and SiO_2, with approximate bulk composition 60 wt% SiO_2 (Table 2), doped at the ppm level with a suite of trace elements using nitrate solutions (Ni, Mn, Co, Zn, Cu, Cd) or SpecPure carbonates (Ca, Sr, Ba). A few milligrams of the
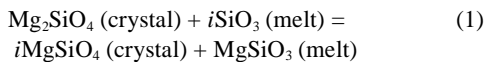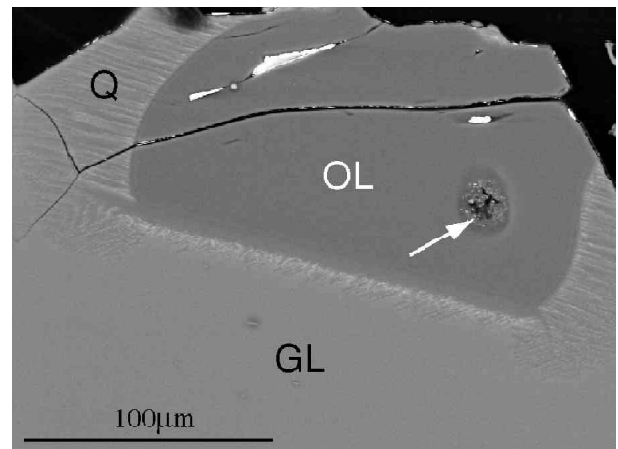
TABLE 1. Short-range potential parameters used in this study. The form of the potential function is $V(r) = A\exp(-r/\rho) - C/r^6$. A charge of $+2.4e$ is assigned to Si, $-1.2e$ to O and $+1.2$ to all other species

ion pair	A (eV)	r (Å)	C (eV Å^6)
Si-O	18003.76	0.2052	133.54
Mg-O	55540.62	0.1665	10.0
Mn-O	12507.99	0.2029	10.0
Ca-O	31513.02	0.2013	10.0
Fe-O	8835.31	0.2055	10.0
Ni-O	128674.43	0.1562	10.0
Co-O	24249.89	0.1818	10.0
Sr-O	22864.25	0.2228	10.0
Cd-O	25513.02	0.2215	10.0
Ba-O	14271.96	0.2491	10.0
O-O	1388.77	0.3623	175.0

FIGURE 1. Backscattered electron micrograph of typical quenched run product. Note that although forsterite (FO) has a thin rind of quench crystal (Q), the matrix itself (GL) is glassy. The black area in the crystal (arrowed) is a pit created by the ion beam during SIMS analysis; small bright areas are residual Au coating.

starting material was run in a Pt capsule in air at 1590 °C for 13 hours, then drop-quenched into water. Quenched run products (crystals of forsterite and quenched glass matrix; Fig. 1) were analyzed with the electron microprobe (EMP) and secondary ion mass spectrometry (SIMS) for major and trace elements, respectively. EMP analyses were performed on C-coated mounts using a 4-spectrometer JEOL JXA-8600 at Bristol University. Si and Mg were analyzed with a 15 kV accelerating voltage and 15 nA beam current; Ca, Fe, Co, Ni, and Zn were analyzed with 20 kV, 50 nA to increase sensitivity. Calibration was carried out on natural and synthetic oxides and minerals. Statistical precision is ±1% relative for major elements, and ±10% for trace elements.

SIMS analyses were performed on Au-coated mounts using a Cameca IMS-4f ion-microprobe at Edinburgh University. The analytical conditions were: primary beam of 10 keV O^- ions; sample current of 8–10 nA focused to a 15–25 μm spot; secondary accelerating voltage of –4500 V; and offset voltage of +77 V with ±20 eV energy window to minimize molecular ion interferences. The following masses were measured: 7, 27, 30, 40, 41, 42, 48, 52, 54, 55, 56, 58, 59, 60, 61, 63, 64, 65, 66, 88, 113, 114, and 138. Electron-multiplier background, monitored at mass 130.5, was always <0.03 cps (and usually zero). The following interferences were explicitly removed by peak-stripping: MgO^+ on ^{40}Ca; $MgSi^+$ on ^{54}Fe and ^{55}Mn; Si_2^+ and CaO^+ on ^{59}Co and ^{60}Ni; Mg_2O^+ and $CaMg^+$ on ^{66}Zn. Statistical precision is better than ±5% relative for all elements in both phases, except for Ba and Cd in olivine (±10%). Partition coefficients were calculated as the ratio of Si-corrected counts in forsterite to glass. This procedure assumes that there are no significant differences in ion-yield between forsterite and $MgO-SiO_2$ glass. Agreement between SIMS and EMP partition coefficients for

elements analyzed by both techniques (Table 2) justifies this approach.

RESULTS AND DISCUSSION

Experimental partition coefficients, including for the first time D_{Cd} and D_{Cu}, are given in Table 2 and plotted alongside calculated values in Figure 2a. Experimental and calculated partition coefficients agree within a factor of 2 for all elements except for the largest elements Sr and Ba, where calculated values are, respectively, under- and overestimated by factors of 4.2 and 3.1. This agreement is remarkable in that the potentials for trace elements used in the simulations are taken straight from their binary oxides *without modification*. Slight differences between experiment and calculation may derive from this simplification. Alternatively, for larger cations such as Sr and Ba, incorporation at extended defects (e.g., Purton et al. 1997b), or trace glass contamination of crystal analyses (e.g., Beattie 1994), may also play a role. For example, during SIMS analysis of our run products, contamination of a forsterite analysis by 1 part in 100 000 of the surrounding glass will increase D_{Ba} by an order of magnitude. The fact that our simulated D_{Ba} underestimates the experimental value supports either of these two possibilities. In any case, the agreement between simulation and experiment is sufficiently strong to warrant confidence in the computational techniques used.

Our results illustrate some deviant partitioning behavior not predicted by the lattice strain model, but reproduced in our simulations. Notably experimental values of D_{Ni}, D_{Cu}, and D_{Zn}, and computer simulated D_{Ni} and D_{Zn}, show that factors other than ionic radius can affect partitioning. To show this, we have fitted the lattice strain model of Blundy and Wood (1994), with a single disordered M-site, to all elements except Co, Ni, Cu, and Zn in order to obtain a "baseline" variation that can be ascribed to ionic radius alone (Fig. 2b). The partition coefficients for Mg, Ca, Mn, Sr, and Ba were fitted to the lattice strain model of Blundy and Wood (1994), using $r_0 = 0.63$ Å, $E = 143$ GPa, $D_0 = 1.7$. The model parameters are in good agreement with observed values for the M-site dimensions and elastic moduli of forsterite at high temperatures, and with previous descriptions of olivine-melt partitioning (Beattie 1994; Hirschmann and Ghiorso 1994). For comparison, the bulk-crystal Young's modulus of forsterite at 1427 °C is 151 ± 2 GPa (Isaak et al. 1989) while the mean M-O and O-O bond lengths in forsterite at 1600 °C are 2.17 ± 0.07 and 3.05 ± 0.28 Å, respectively (Takeuchi et al. 1984). Beattie (1994) fitted his olivine-melt partitioning data, using a slightly different procedure, with $r_0 = 0.58$ Å, and $E = 151$ GPa.

The experimental value of D_{Ni} is higher than would be predicted from its ionic radius alone, whereas D_{Cu} and D_{Zn} are lower (Fig. 2b). The high value for Ni is well documented (e.g., Beattie et al. 1991; Hirschmann and Ghiorso 1994), and is in keeping with the significant crystal field stabilization energy (CFSE) for Ni^{2+}, which imparts a preference for the octahedral crystal site over the more-distorted, and probably lower-coordination environment in the melt (Kubicki and Lasaga 1991; Brown et al. 1995; George and Stebbins 1998). The magnitude of this CFSE effect, however, is small, amounting to a reduction of no more than 10 kJ/mol in the lattice strain energy. This finding is

TABLE 2. Composition of starting material, and forsterite-melt partition coefficients determined by computer simulation and from experiment

| Element | Starting material† | Partition coefficients* | | |
		EMP	SIMS	Simulation
Li	4.83(7)	na	0.083(9)	nc
Mg	22.7(12)×10⁴	1.550(11)	na	1.43‡
Al	226(17)	na	0.10(8)	nc
Si	27.3(1)×10⁴	0.723(4)	norm	0.71‡
Ca	4680(150)	0.024(5)	0.217(4)	0.011
Fe^{3+}		0.30(7)	0.14(3)	nc
Mn	*50*	na	0.41(5)	0.29
Co	*100*	0.9(8)	1.09(5)	1.0
Ni	*50*	2.0(9)	2.65(18)	1.7
Cu	*400*	na	0.17(6)	nc
Zn	*1000*	0.55(17)	0.36(6)	0.84
Sr	5540(520)	na	1.04(7)×10⁻⁴	2.5×10⁻⁵
Cd	*3000*	na	0.082(15)	0.10
Ba	2.30(12)×10⁴	na	1.3(7)×10⁻⁶	4.0×10⁻⁶

* Partition coefficients (*D*) are weight fraction in crystal/weight fraction in glass. Simulated values are calculated from ΔH_{ex} using Equation 3. Experimental values are determined by EMP and SIMS analysis. na = not analyzed; nc = not calculated; norm = element used for normalisation of SIMS analysis. Figure in parentheses is 1 standard deviation based on *n* analyses of crystals (*n* = 6) and glass (*n* = 5) and expressed in terms of last significant digit(s).
† Units ppm by weight. Determined by EMP analysis of starting material fused at 1600 °C for 12 hours, except for those values in italics which denote weighed-in concentration. Li, Fe^{3+}, and Al are present as trace contaminants.
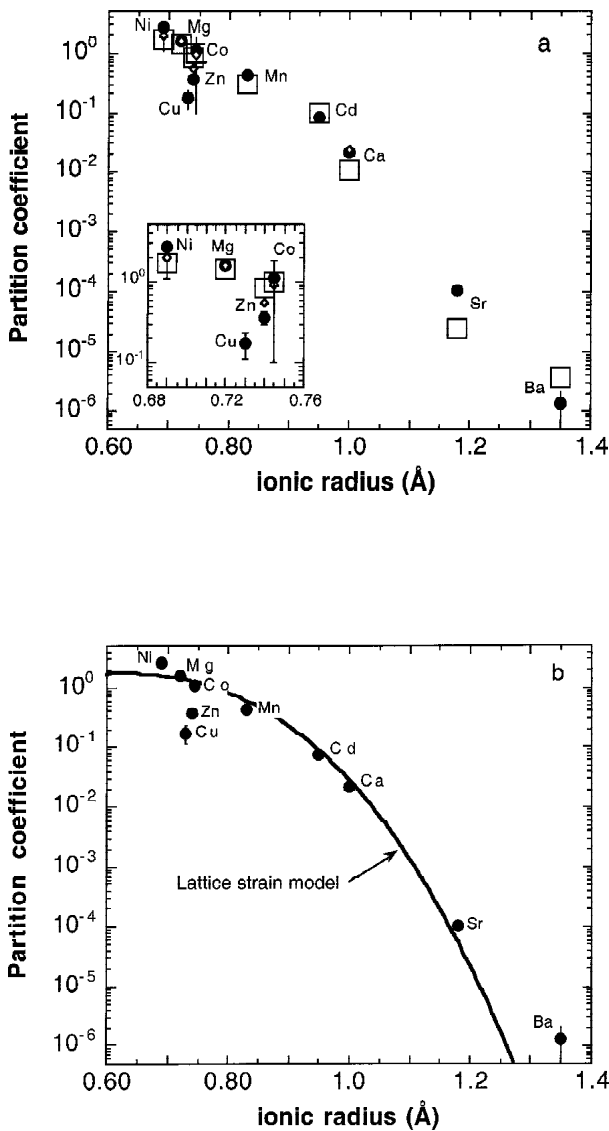‡ Input values.

FIGURE 2. (**a**) Comparison of calculated and experimental forsterite-melt partition coefficients in the system MgO-SiO$_2$ at 1600 °C. Partition coefficients are shown for MC calculation (open squares), SIMS analysis of experimental run products (filled circles), and EMP analysis of experimental run products (filled diamonds), and are plotted against ionic radius (Å) in sixfold coordination (Shannon 1976). The agreement between experimental and simulated partition coefficients, over the observed extreme variation, endorses our new computational approach. (**b**) Deviant partitioning behavior of selected cations relative to that predicted from ionic radius alone. Line shows lattice strain model fit to the experimental data (SIMS values only, open circles), excluding Co, Ni, Cu, and Zn (parameters given in text). Misfit for Ba probably reflects analytical artifacts or non-equilibrium effects, as described in the text (cf., Beattie 1994). For the excluded elements, deviant behavior indicates either a preference for the crystal (Ni) or for the melt (Cu, Zn), which can be rationalized in terms of CFSE and melt structure, respectively. Note that the partition coefficient of Cd is consistent with its similar ionic radius to Ca, despite being in the same Group as Zn.

at odds with claims that for Ni^{2+} the CFSE *alone* controls partitioning (Keppler 1992). The simulations take some account of crystal field stabilization energy in that the Ni-O potential was obtained by fitting to the lattice parameter of NiO, in which the Ni^{2+} ion is in an octahedral environment. However, since the same potentials are used for both mineral and melt, the simulations do not allow for any *difference* in CFSE between solid and melt. This is a possible reason why the simulations underestimate D_{Ni}. The analogous CFSE contribution for Co^{2+} appears sufficiently small (Fig. 2b) and can be neglected.

In contrast to Ni, low experimental values of D_{Cu} and D_{Zn} indicate that these cations prefer the distorted structure of the melt phase. This finding is consistent with the fact that of all the elements investigated, it is only these two that do not form cubic oxides at zero pressure. Due to the Jahn-Teller effect, Cu^{2+} prefers structures with unusual co-ordination geometries, perhaps more akin to those found in the melt than in the crystal. This effect is somewhat larger than that for Ni^{2+}, amounting to an increase of ~30 kJ/mol in the crystal lattice strain energy. Two-body potential models of the type used here cannot allow for Jahn-Teller distortions and so we have not performed any simulations for Cu^{2+}. Zn^{2+} also appears to show a preference (~20 kJ/mol) for a lower-coordination site in the melt. The calculated value of D_{Zn}, based upon potentials derived for ZnO, in which Zn is in fourfold rather than sixfold coordination with O, shows the same behavior as the experimental values. We note from Figure 2b that, in both experiment and simulation, Cd^{2+}, a larger ion also in Group IIB, but forming a cubic oxide, behaves like any divalent cation of similar radius (e.g., Ca^{2+}).

Our principal finding is that atomistic computer simulations can be used to calculate crystal-melt partitioning at high temperature. Such calculations are low cost compared with experiments, and therefore provide a highly valuable adjunct to experimental studies, especially when conditions present extreme technical difficulties, for example, at very high pressures. Further refinement of our computational technique is now required in order to build in the effects of pressure, and of charge compensation, which is important when considering the partitioning of heterovalent cations, such as the lanthanides or alkali metals.

REFERENCES CITED

Beattie, P. (1994) Systematics and energetics of trace-element partitioning between olivine and silicate melts: Implications for the nature of mineral/melt partitioning. Chemical Geology, 117, 57–71.
Beattie, P., Ford, C., and Russell, D. (1991) Partition-coefficients for olivine-melt and orthopyroxene-melt systems. Contributions to Mineralogy and Petrology, 109, 212–224.
Blundy, J.D. and Wood, B.J. (1994) Prediction of crystal-melt partition coefficients from elastic moduli. Nature, 372, 452–454.
Bowen, N.L. and Andersen, O. (1914) The binary system MgO-SiO$_2$. American Journal of Science (4th ser.), 37, 487–500.
Brenan, J.M., Shaw, H.F., Ryerson, F.J., and Phinney, D.L. (1995) Experimental determination of trace-element partitioning between pargasite and a synthetic hydrous andesitic melt. Earth and Planetary Science Letters, 135, 1–11.
Brice, J.C. (1975) Some thermodynamic aspects of the growth of strained crystals.

Journal of Crystal Growth, 28, 249–253.

Brown, G.E. Jr., Farges, F., and Calas, G. (1995) X-ray scattering and X-ray spectroscopy studies of silicate melts. In Mineralogical Society of America Reviews in Mineralogy, 32, 317–410.

Catlow, C.R.A and Price, G.D. (1990) Computer modelling of solid-state inorganic materials. Nature, 347, 243–248.

Frenkel, D. and Smit, B. (1996) Understanding Molecular Simulation, 443 p. Academic Press, San Diego, U.S.A.

George, A.M. and Stebbins, J.F. (1998) Structure and dynamics of magnesium in silicate melts: A high-temperature ^{25}Mg NMR study. American Mineralogist, 83, 1022–1029.

Goldschmidt, V.M. (1937) The principles of distribution of chemical elements in minerals and rocks. Journal of the Chemical Society (London), 655–673.

Hirschmann, M.M. and Ghiorso, M.S. (1994) Activities of nickel, cobalt and manganese silicates in magmatic liquids and applications to olivine liquid and to silicate metal partitioning. Geochimica et Cosmochimica Acta, 58, 4109–4126.

Isaak, D.G., Anderson, O.L., Goto, T., and Suzuki, I. (1989) Elasticity of single-crystal forsterite measured to 1700 K. Journal of Geophysical Research, 94, 5895–5906.

Keppler, H. (1992) Crystal-field spectra and geochemistry of transition metal ions in silicate melts and glasses. American Mineralogist, 77, 62–75.

Klein, M., Stosch, H.G., and Seck , H.A. (1997) Partitioning of high field strength and rare-earth elements between amphibole and quartz-dioritic to tonalitic melts: An experimental study. Chemical Geology, 138, 257–271.

Kubicki, J.D. and Lasaga, A.C. (1991) Molecular dynamics simulations of pressure and temperature effects on $MgSiO_3$ and Mg_2SiO_4 melts and glasses. Physics and Chemistry of Minerals, 17, 661–673.

Lundstrom, C.C., Shaw, H.F., Ryerson, F.J., Williams, Q., and Gill, J. (1998) Crystal chemical control of clinopyroxene-melt partitioning in the Di-Ab-An system: Implications for elemental fractionations in the depleted mantle. Geochimica et Cosmochimica Acta, 62, 2849–2862.

Metropolis, N., Rosenbluth, M.N., Teller, A.H., and Teller, E. (1953) Equation of state calculations by fast computing machines. Journal of Chemical Physics, 61, 1087–1092.

Nagasawa, H. (1966) Trace element partition coefficients in ionic crystals. Science, 152, 767–769.

Purton, J.A., Allan, N.L., Blundy, J.D., and Wasserman, E.A. (1996) Isovalent trace element partitioning between minerals and melts—a computer simulation study. Geochimica et Cosmochimica Acta, 60, 4977–4987.

Purton, J.A., Allan, N.L., and Blundy, J.D. (1997a) Calculated solution energies of heterovalent cations in forsterite and diopside: Implications for trace element partitioning. Geochimica et Cosmochimica Acta, 61, 3927–3936.

Purton, J.A., Allan, N.L., and Blundy, J.D. (1997b) Impurity cations in the bulk and the {001} surface of muscovite. Journal of Materials Chemistry, 7, 1947–1951.

Redfern, S.A.T., Henderson, C.M.B., Knight, K.S., and Wood, B.J. (1997) High-temperature order-disorder in $(Fe_{0.5}Mn_{0.5})_2SiO_4$ and $(Mg_{0.5}Mn_{0.5})_2SiO_4$ olivines: An in situ neutron diffraction study. European Journal of Mineralogy, 9, 287–300.

Shannon, R.D. (1976) Revised effective ionic radii and systematic studies of interatomic distances in halides and chalcogenides. Acta Crystallografica, A32, 751–767.

Takeuchi, Y., Yamanaka, T., Haga, N., and Hirano, M. (1984) High temperature crystallography of olivines and spinels. In I. Sunagawa, Ed., Materials Science of the Earth's Interior, p. 191–231. Terra Scientific Publishing, Tokyo.

Taura, H., Yurimoto, H., Kurita, K., and Sueno, S. (1998) Pressure dependence of partition coefficients for trace elements between olivine and the coexisting melts. Physics and Chemistry of Minerals, 25, 469–484.

Van Westrenen, W., Blundy, J.D., and Wood, B.J. (1999) Crystal-chemical controls on trace element partitioning between garnet and anhydrous silicate melt. American Mineralogist, 84, 838–847.

Wood, B.J. and Blundy, J.D. (1997) A predictive model for rare earth element partitioning between clinopyroxene and anhydrous silicate melt. Contributions to Mineralogy and Petrology, 129, 166–181.